Payri Marín, R.; Salvador Rubio, FJ.; Marti Aldaravi, P.; Martínez López, J. (2012). Using one-dimensional modeling to analyse the influence of the use of biodiesels on the dynamic behavior of solenoid-operated injectors in common rail systems: Detailed injection system model. Energy Conversion and Management. 54(1):90-99. doi:10.1016/j.enconman.2011.10.004.

Energy Conversion and Management 54 (2012) 90–99

USING ONE-DIMENSIONAL MODELLING TO ANALYSE THE INFLUENCE OF THE USE OF BIODIESELS ON THE DYNAMIC BEHAVIOR OF SOLENOID- OPERATED INJECTORS IN COMMON RAIL SYSTEMS: DETAILED INJECTION SYSTEM MODEL.

R. Payri, F. J. Salvador (*), P. Martí-Aldaraví, J. Martínez-López

CMT-Motores Térmicos. Universitat Politècnica de València, Spain

Camino de Vera s/n, E-46022 Spain

(*) Corresponding author:

Dr. F. Javier Salvador, fsalvado@mot.upv.es

CMT-Motores Térmicos, Universitat Politècnica de València

Camino de Vera s/n, E-46022 Spain.

Telephone: +34-963879658

FAX: +34-963877659

ABSTRACT

A combined experimental and computational investigation has been performed in order to evaluate the influence of physical properties of biodiesel on the injection process in a common-direct injection system with second generation solenoid injectors. For that purpose, after a complete characterization of the system, which involved mechanical and hydraulic characterization, a one-dimensional model has been obtained and extensively validated. Simulations have then been performed with a standard Diesel and a 100% rape methyl ester (RME) biodiesel which allowed a comparison and analysis of the dynamic response of the injector to be done. Different injection strategies involving main injection and main plus post-injection have been used to explore the impact of the use of biodiesel on the performance and stability of solenoid injectors.

As far as the dynamic response of the injector is concerned, the results obtained have clearly shown that the use of biodiesel affects the dynamic response of the needle, especially at low injection pressures. The behavior of the system under multi-injection strategies (main plus post injection) has been also evaluated determining for different operating conditions (injection pressures and backpressures) the minimum dwell time between injections to assure a stable behavior in the injection process (mass flow rate). Important differences have been found between biodiesel and standard diesel in this critical parameter at low injection pressures, becoming less important at high injection pressure. Finally, a modification on the injector hardware has been proposed in order to compensate these differences.

KEYWORDS: injector, modelling, biodiesel, Diesel, dynamic

NOMENCLATURE

A_o	Geometrical area
C_c	Contraction coefficient
C_d	Discharge coefficient
CN	Cavitation number
D_o	Geometrical nozzle diameter
K	Cavitation number
$\dot{m}_f$	Mass flow
P_b	Discharge pressure
P_{inj}	Injection pressure
P_v	Vapor pressure
u_B	Theoretical velocity, $u_B = \sqrt{\frac{2 \cdot \Delta P}{\rho_l}}$
U_o	Outlet velocity

Greek Symbols

ΔP	Pressure drop, $\Delta P = P_{inj} - P_b$
ρ_f	Fuel density
υ_f	Kinematic viscosity

Subscripts

crit Critical conditions

1. INTRODUCTION

The use of biodiesels is receiving an increasing interest as a substitute for fossil fuels in internal combustion engines [1]. Several recent studies on diesel engines have revealed that the use of biodiesel can reduce unburned hydrocarbon (HC), soot emissions and carbon monoxide (CO) emission while relating a small NOx increase [2], [3], [4], [5], [6], [7], [8], [9], [10]. Most of these studies treat the engine as a "black box" comparing standard fuel and biodiesel (pure or blended) mainly in terms of emissions, concluding on important reductions. Nevertheless, there are few studies dealing with the impact of physical properties of biodiesel on the injection process [11], [12]. In fact, the use of biodiesel could have clear consequences on the injection system operation. In overall terms, biodiesel fuels are produced from transesterification of vegetable oil, and can be used pure or blended as a substitute for diesel fuel. Normally they present higher density and viscosity than standard diesel. Higher density would mainly imply higher mass flow rate provided by the injection system at stationary conditions (at a given injection pressure, and at maximum injector needle lift conditions). Nevertheless, the higher viscosity of biodiesels can affect the dynamic behavior of the system (especially of the injector), slowing down the opening and closing of the injector needle, and also affecting the flow regime (Reynolds number), and so the discharge coefficient of calibrated orifices and nozzles orifices. As a direct consequence of that, viscosity can also have a negative effect on multiple injections stability, affecting the time needed between injections (dwell times) to operate in stable way. Pressure wave's frequency in the injector pipes could be also influenced by the use of biodiesel according to its different speed of sound, which in turn depends on the density and bulk modulus.

As mentioned above, studies aiming at analyzing all these phenomena are scarce and they are not being completely addressed yet.

In the present investigation a combined experimental and computational study has been performed in order to evaluate the influence of physical properties of biodiesel on the injection process in a common-direct injection system with second generation solenoid injectors. To achieve this objective, firstly a one-dimensional model has been obtained and extensively validated with experimental data. The choise of a one-dimensional model seems to be the best way to deal this kind of problems because it provides us with the chance of studying the internal hydro-dynamic behavior of the injector which is difficult otherwise.

The description of the injector characterization and the one-dimensional modelling methodology are dealt with in a first paper (the present one). Then, in a second part of the study, simulations have been performed with a standard Diesel and a 100% rape methyl ester (RME) biodiesel which allowed a comparison and analysis of the dynamic response of the injector to be done with simple and multiple injections strategies.

The outline of the present article is the following:

After this introduction, in section 2, the experimental facilities used for the injector characterization are described. The proposed methodology for modeling the injection system is based on two different types of characterization: a detailed dimensional characterization and a hydraulic characterization of the different internal parts of the injectors. For the dimensional characterization a fine detail measuring technique applied to all the internal constituents of the injector is used. Dimensional measurements include the passages and internal lines of the injector, internal volumes, calibrated orifices, springs, clearance between moving parts, etc. The hydraulic characterization

makes reference mainly to the characterization of the mass flow at different pressure conditions for all the calibrated orifices (either in the nozzle or in the control volume), which together with dimensional information allows the discharge coefficient to be determined as a function of the pressure drop. In section 3, the model description is performed. The model of the injector is divided into three parts: injector holder, nozzle and electrovalve. Finally, in section 4 the validation is carried out. The validation of the model is performed by comparing the mass flow rates provided by the model with those obtained experimentally by means of a mass standard injection rate discharge curve indicator (IRDCI) based on Bosch method.

2. EXPERIMENTAL TOOLS

The experimental tools used for the dimensional and hydraulic characterization of the injection system are as follows:

1. Silicone moulds and scanning electron microscope (SEM).
2. Hydraulical characterization test rigs.
3. Injection rate test rig.

2.1 Silicone moulds and scanning electron microscope (SEM)

In order to analyse the internal characteristics of the injector, such as volumes, control calibrated orifices, nozzle orifices and other channels of the injector, a methodology based on the use of silicone moulds and their visualization in a SEM microscope has been used [13]. Images taken with the microscope are processed with the help of a computer aided design (CAD) software. Pictures of the specific geometries obtained using the electronic microscope come with a reference dimension. With this reference

dimension it is possible to load the pictures in the CAD software with the appropriate scale factor and from this point obtain accurate dimensions of the part of the injector being characterized. This methodology is applicable when determining the geometry of the volumes and internal channels as well as the dimensions of the control and nozzles orifices. An example of this methodology is shown in Figure 1, where the silicone moulds of the internal part of the piece containing the control inlet orifice and control outlet orifice are shown. From that figure, it can be seen that the inlet diameter is 220 micrometers and the outlet diameter is around 246 micrometers.

2.2 Hydraulical characterization test rigs

The objective of the hydraulical characterization test rigs is to characterize all internal calibrated orifices in order to determine their discharge coefficient as a function of the pressure drop, or more specifically of the Reynolds number. Such information is of great importance for modeling purposes and has to be determined with high level of accuracy to ensure a good model behavior.

They are used to characterize either the nozzle orifices or the control volume orifices. In the case of the nozzles orifices, the test rig depicted in Figure 2 is used. In this facility, the nozzle is mounted in a nozzle holder which is completely empty to avoid any friction loss different from that of the nozzle orifices. Even the needle of the nozzle is removed. The injection pressure (P_{inj}) is generated and controlled by a standard common rail injection system [14]. The nozzle injects into the discharge chamber where the backpressure (P_b) is controlled by means of a valve.

In Figure 3, the results from the hydraulical characterization of the nozzle are depicted. In that figure, the flow rate is represented against the squared root of the pressure drop, for four injection pressures (10, 20, 50 and 80 MPa) and different levels of

backpressure. As it can be seen from the figure, mass flow rate increases linearly with the square root of the pressure drop, which is an expected result taking into account that, as will be pointed out in section 3.2, the orifice of the nozzles has an important degree of convergence, and so, cavitation inside is avoided [13], [15], [16].

Once the mass flow rate is obtained for each of the pressure conditions, it is possible to obtain the discharge coefficient combining Bernoulli´s equation and mass conservation equation.

Mass conservation equation leads to:

$$\dot{m}_f = C_d \cdot A_o \cdot \rho_f \cdot u_B \tag{1}$$

where $\dot{m}$ is the mass flow rate, ρ_f represents the liquid density, A_o is the geometrical cross section of the orifice which is determined by the technique based on silicone moulds and their subsequent visualization as previously described in point 2.1. The term u_B is the bernoulli´s theroretical velocity which can be represented as a function of the injection pressure and backpressure as:

$$u_B = \sqrt{\frac{2 \cdot (P_{inj} - P_b)}{\rho_f}} \tag{2}$$

and, therefore, the discharge coefficient can be easily obtained combining equations (1) and (2):

$$C_d = \frac{\dot{m}_f}{A_o \cdot \sqrt{2 \cdot \rho_f \cdot (P_{inj} - P_b)}} \tag{3}$$

In Figure 4, the discharge coefficient is depicted against the theoretical Reynolds number. The Reynolds number is calculated as:

$$\mathrm{Re} = \frac{D_o \cdot U_o}{\upsilon_f} \tag{4}$$

Where $D_{o,}$ is the outlet diameter, υ_f is the kinematic viscosity of the fuel, and U_o is the velocity at the orifice outlet. If the Bernoulli´s theoretical velocity is taken instead of the actual velocity, the Reynolds number can be considered as a theoretical Reynolds number. This figure shows how the discharge coefficient increases when the Reynolds number increases. This increase is continuous and has an asymptotic theoretical maximum value (for an infinite Reynolds number). As outlined by other researchers in the literature, the variation law for the discharge coefficient with the Reynolds number depends strongly on the orifice geometry [13],[17],[18],[19],[20]. In Figure 4, a correlation for the discharge coefficient as a function of Reynolds number obtained from the experimental data has also represented. The same type of equation was used and justified by the authors in Payri et al. [13]. The R-squared value obtained for the correlation is around 98%, which represents a high level of confidence.

Apart from the nozzle orifices, there are also two calibrated orifices which play an important role in the injector operation: the inlet orifice and the outlet orifice of the control volume which have been dimensionally characterized in Figure 1 as a example of the silicone technique. As can be seen from that figure, they are drilled in a piece containing both. To perform the hydraulical characterization of them, a special test rig with two different configurations, depending on the orifice to be analysed, has been used. These configurations are shown in Figure 5. Both set ups are conceived to force the fluid to pass through the orifice to be characterized and with the same hydraulic path

as it takes place in actual injector operation. So that, for characterizing the inlet control orifice (Figure 5a) the fluid supplied by a high pressure pump passes through the inlet orifice where the feed pressure is controlled, and it exits through the lower part which is connected to a volume where the backpressure is also controlled. For the characterization of the outlet orifice (Figure 5b), the test rig is fed from the lower part where the feed pressure is controlled. The flow passes through the outlet orifice which is connected to a volume where the control of the backpressure is carried out.

As in the case of the nozzle, in order to carry out the tests at different pressure drops (i.e. different Reynolds number), tests are conducted at different values of inlet pressure, for which the pressure at the outlet is varied between a minimum value of 0.1 MPa and the inlet pressure. After a short stabilization time, when steady flow conditions are achieved, the mass flow rate across the orifice is measured. Figure 6 shows the results obtained for the inlet and outlet control orifices. The mass flow rate as a function of the square root of the pressure difference is depicted in the Figure. The experiment was carried out for two injection pressures, 10 and 20 MPa, and the discharge pressure was varied from these values to the atmospheric pressure. Since both control orifices are cylindrical, cavitation is expected to occur [13],[15],[16],[20]. In fact, the values of the pressure difference at which the choking of the mass flow rate occurs is closely related with the onset of cavitation [21]. These points are identified in the figure by vertical dotted lines, one for each injection pressure. These conditions are called critical cavitation conditions. Cavitation regimen in an injector can be represented by using some of the different cavitation numbers proposed in the literature. These are non-dimensional parameters that make it possible to establish whether the relevant flow conditions in the injector nozzle, that is to say, the pressure difference, are favourable or not to the occurrence of cavitation. Definitions of this parameter vary throughout the

literature, but they are mainly based on the pressure difference across the injector orifice. In this work, the cavitation number definition used by Soteriou et al. [22] is considered:

$$CN = \frac{P_{inj} - P_b}{P_b - P_v} \tag{5}$$

where P_v is the saturation vapor pressure which is often neglected in the equation because of its small value in comparison to the injection pressure or the backpressure.

For cavitating nozzles, the critical cavitation number is defined as CN_{crit}, corresponding to the pressure drop for which cavitation starts in the nozzle orifice. This phenomenon occurs at a given value of the injection, and it is detected by the stabilization of the mass flow rate across the orifice, in spite of the further decrease in discharge pressure. Hence, cavitation will not be produced unless the cavitation number corresponding to these pressure conditions is higher than the critical value, $CN_{crit.}$ In the present case, the critical cavitation numbers found for the inlet orifice at 10 MPa and 20 MPa are CN_{crit}= 2.4 and CN_{crit}= 2, respectively. For the outlet orifice, the critical cavitation numbers are CN_{crit}= 4.82 and CN_{crit}= 4.17, respectively. These values can be easily obtained from the information given in Figure 6.

When the orifices do not cavitate, the discharge coefficient presents the same behavior as shown in Figure 4 (increasing trend with Reynolds number). Nevertheless, under cavitating conditions, which can be achieved by increasing the pressure difference, the discharge coefficient only depends on the cavitation number, not longer on the Reynolds number ([13], [22], [23], [24]), following the equation:

$$C_d = C_c \cdot \sqrt{1 + \frac{1}{CN}} \tag{6}$$

where C_c is the contraction coefficient in the orifice owing to cavitation phenomena which can be easily obtained particularizing that equation for the critical cavitation conditions, CN_{crit} at which the discharge coefficient is known. Obviously, equation (6) is only valid for $CN>CN_{crit}$.

2.3 Mass flow rate characterization

The injection rate test rig allows make it possible to take measurements of injection rate in order to compare with the models results. This allows the obtained model to be validated. Mass flow rate measurements for validation purposes have been performed in a standard injection rate discharge curve indicator (IRDCI), based on Bosch method [14]. This installation measures the pressure increment produced by the discharged fuel on a fuel-filled tube, which is directly related with the amount of fuel injected. By this way, information about instantaneous mass flow given by the nozzle along the whole injection process is obtained. The whole system is controlled by a Genotec impulse generator, simulating the function of the ECU (Electronic Control Unit). The fuel used was a Repsol CEC RF-06-99. The main properties of this fuel are reported in Table 1.

Three injections pressure values, controlled at the rail, were used: 30, 80 and 130 MPa. The back pressure used was 4 MPa. For all the pressure values, four injector energizing times were considered: 0.24, 0.5, 1 and 2 ms. The mass flow rates obtained for those injection conditions will be shown in Section 4 where the validation of the model is done by comparing the mass flow rates given by the model with those experimentally characterised.

3. MODEL DESCRIPTION

For the model, the commercial integrated platform for 1D system simulation, AMESim was used [25]. Within this platform, to create a simulation model for the injection system a set of validated libraries can be used, containing pre-defined components for different physical domains. The components are described using validated analytical models that represent the injection system actual hydraulic, mechanic and electric behavior.

The proposed model has been divided into three parts: the injector nozzle, the injector holder and the electrovalve, connected mechanically and hydraulically, as described below.

3.1 Model of the injector holder

The proposed model of the injector holder is shown in Fig. 7. In this model a pressure source is considered, simulating the pump. This pressure source feeds a volume of 20 cm^3 which represents the rail. The rail is connected to the injector holder with a high pressure line (HPL1). At the entrance of the injector holder there is a restriction simulating the edge filter. Following, there is a separation into two lines. The first feeds directly to the nozzle (through lines L2, L3 and L4). The second line feeds the upper part of the injector, through the volume V1, the control volume inlet orifice (orifice OZ) and finally the volume V2 where the upper part of the rod is located. The conical section in the upper part of the road has been modelled by a conical valve which fits very well to the actual shape of the upper part of the rod and which effective pressure section varies with the rod lift. Moreover, and additional piston taking into account the pressure force acting on the flat part of the upper part of the rod is considered (VP3). Following the conical valve (OV1) the volume V2 is located, which precedes the

control volume outlet orifice (OA), the opening of which is controlled by the command piston of the electrovalve. After this orifice, the return channel is located. The values of the parameters used to define these elements can be seen in Table 2.

For the characterization of volume 2 and volume 3 (V2 and V3), photographs taken with the electronic microscope of the silicone mould were used (Figure 8, at the bottom). These photographs together with photograph of the upper part of the rod make it possible to determine volumes 2 and 3.

3.2 Model of the nozzle.

Figure 9, on the right, shows a scheme of the nozzle with the different internal lines and volumes. The most important part from the point of view of the model is the configuration of the needle seat. In the same figure, on the left, the proposed model of the nozzle is shown. This model is connected to the model of the injector holder by means of a hydraulic connection (NL1) and a mechanical connection (mechanical contact between needle and rod). In the upper part of the nozzle there is the line NL1, feeding the volume NV1, connected to the piston NP1, which allows the simulation of the action of the pressure force in the upper part of the needle. Following the volume NV1, there is the line NL2 with a section equivalent to the clearance between the needle and the internal part of the nozzle where the needle is placed. This line feeds the volume NV2 which is associated with the piston NP2 that simulate the existing volume between the needle and its seat and the crown under the action of pressure force. The volume NV2 also feeds the valve with conical seat (OV3) simulating the tip of the needle and its seat. Following the conical valve, the volume NV3 connected with the 6 discharge orifices is placed. A summary of the main parameters involved with these elements can be seen in Table 3.

For the dimensional characterization of all these volumes and the geometric sections of the different pistons considered in the model, the superposition of a photograph of the needle and a photograph of the silicone mould of the seat (including orifices) was used, as shown in Figure 10. In this figure, the photograph of the needle with dimensions marks is shown on the left, the photograph of the nozzle mould with the six-orifices is depicted in the middle, and finally, the superposition of these two photographs allows the characterization of volumes NV2 and NV3. The conical seat (OV3) and the two pistons considered are mechanically connected to the needle mass (NM) which in turns is connected to a fictitious spring, which actually does not exist but makes it possible to model the deformation of the needle that is caused by the pressure forces at the extremes of the needle.

As with the inlet and outlet orifices of the control volume, one of the most critical aspects for modeling the nozzle is the characterization of the discharge orifices dimensionally as well as hydraulically. In this case, through the use of the silicone method, the most important dimensions of the needle seat can be found as well as the diameter of the orifices. From the point of view of the one-dimensional model, the most important parameters are the number of orifices and their respective diameters, since they define the permeability (discharge capacity) of the nozzle. For the nozzle characterized, the diameter of the six orifices was determined. The mean value was 131 μm, with a standard deviation of ±2μm.

As far as the hydraulical characterization is concerned, the discharge coefficient previously characterized in section 3 (Figure 4), is the most important parameter that the model needs.

3.3 Model of the electrovalve

Figure 11, at the upper part on the left, shows a physical scheme of the electrovalve and on the right a zoom of the magnetic path is shown. At the bottom, the model created with the code is depicted. The moving element of the electrovalve is the command piston, labeled as AM in the picture. The ascending movement of the command piston owing to the electric current of command opens the outlet orifice of the control volume by displacing the small sphere. Therefore, the displacement signal of the command piston is the only connection that exists with the model of the injector holder. The spring BS opposes the opening of the control piston and maintains the piston and the small sphere closing the outlet (OA, in Figure 8) while there is no excitation current.

The electrovalve is feed by a voltage signal which is the input of the variable voltage source (U). This signal is a reproduction of that provided by the ECU for a given energizing time of the injector. The voltage source is connected to an electric coil with 32 coils. The current in the electric circuit induces a flux in the magnetic circuit. The magnetic flux passes through the actuator core (MC1, MC2 and MC3), the upper part of the command piston (MC4 or induced, IND) and the air-gap (AG). Elements MC1 and MC3 are longitudinal magnetic elements while elements MC2 and IND are radial magnetic elements. The reluctances of them depend on the material, and length and effective magnetic areas have been estimated from the dimensional analysis. The values of the most important parameters of the electrovalve are summarized in Table 4.

4. MODEL VALIDATION

A complete sketch of the model involving the different parts described y previous section is shown in Figure 12.

In order to validate the model, several experimental measurements were performed using the injection rate test bench previously described. The experimental measurements correspond to rail pressures of 30, 80 and 130 MPa. For each of these pressures, four different durations of electrical pulses are used: 240, 500, 1000 and 2000 μs. In Figure 13, the experimental mass flow rates are compared with those obtained from the model for all injection pressure conditions and energizing times. In the Figure 14, the total amount of fuel mass of the model and the experimental measurements are also compared for the 11 points tested. Both figures show up the ability of the model to predict the experimental results with quite high level of accuracy both in terms of mass flow rate shape (Figure 13) and in total mass injected (Figure 14) where the maximum deviations found are lower than 6%.

5. CONCLUSIONS

This research presents a methodology for modeling standard common rail diesel injection systems. This methodology is based on two types of characterization:

1. A dimensional characterization of all the internal parts of the injector. Apart from basic metrology, this characterization is based on the acquisition of silicone moulds, and then the visualization of them in an electronic microscope.

2. A hydraulical characterization of the orifices and internal elements of the injector (mainly nozzle and control orifices)

With this information and the help of a one-dimensional calculation code, a model of this system has been created and validated. The comparison of the injection rate proportionated by the model with the experimental data for different injection

conditions shows a good performance of the model and therefore the ability of it to predict the injection rate with high level of accuracy.

ACKNOWLEDGMENTS

This research has been funded by “Ministerio de Ciencia e Innovación” in the frame of the project “Estudio teórico experimental de la influencia del combustible sobre la cavitación y el desarrollo del chorro evaporative (FlexiFuel)”, Reference TRA2010-17564.

This support is gratefully acknowledged by the authors.

REFERENCES

[1]. J.M. Luján, B. Tormos, F.J. Salvador, K. Gargar, Comparative analysis of a DI diesel engine fuelled with biodiesel blends during the European MVEG-A cycle: Preliminary study, Biomass Bioenerg. 33 (2009) 941-947.

[2]. A. Senatore, M. Cardone, M. Buono, V. Rocco, Combustion study of a common rail diesel engine optimized to be fueled with biodiesel, Energ. Fuel 22(3) (2008) 1405-1410.

[3]. M. Lapuerta, O. Armas, J. Rodríguez-Fernández, Effect of biodiesel fuels on diesel engine emissions, Prog. Energy Combust. Sci. 34 (2008) 198-223.

[4]. K.F. Hansen, M.G. Jensen, Chemical and biological characteristics of exhaust emissions from a DI Diesel engine fuelled with rapessed oil methyl esther (RME). SAE Paper 971689 (1997).

[5]. X. Shi, Y. Yu, H. He, S. Shuai, J. Wang, R. Li, Emission characteristics using methyl soyate-ethanol-diesel fuel blends on a diesel engine, Fuel 84 (2005) 1543-1549.

[6]. A. Monyem, J.H. Van Gerpen, The effect of biodiesel oxidation on engine performance and emissions, Biomass Bioenerg. 20 (2001) 317-325.

[7]. Ozsezen Ahmet Necati, Canackci Mustafa, Determination of performance and combustion characteristics of a diesel engine fueled with canola and waste palm oil methyl esters, Energ. Convers. Manage. 50 (2011) 153-162.

[8]. Qi D. H., Chen H., Geng L. M.; et al., Experimental studies on the combustion characteristics and performance of a direct injection engine fueled with biodiesel/diesel blends, Energ. Convers. Manage. 51 (2010) 2985-2992.

[9]. Lin Chern-Yuan; Chiu Chu-Chiang, Burning characteristics of palm-oil biodiesel under long term storage conditions, Energ. Convers. Manage. 51 (2010) 1464-1467.

[10]. Hamdan M. A., Khalil Runa Haj, Simulation of compression engine powered by Biofuels, Energ. Convers. Manage. 51 (2010) 1714-1718.

[11]. F. Boudy, P. Seers, Impact of physical properties of biodiesel on the injection process in a common-rail direct injection system, Energ. Convers. Manage. 50 (2009) 2905-2912.

[12]. A.L. Boehman, D. Morris, J. Szybist, E. Esen, The impact of the Bulk Modulus of Diesel fuels on Fuel Injection Timing. Energ. Fuel 18 (6) (2004) 1877-1882.

[13]. F. Payri, V. Bermúdez, R. Payri, F.J. Salvador. The influence of cavitation on the internal flow and the Spray characteristics in diesel injection nozzles. Fuel 83 (2004) 419-431.

[14]. R. Payri, F.J. Salvador, J. Gimeno, G. Bracho. A new methodology for correcting the signal cumulative phenomenon on injection rate measurements. Exp. Techniques, 32-1 (2008) 46-49.

[15]. F.J. Salvador, J.V. Romero, M.D. Roselló, J. Martínez-López, Validation of a code for modelling cavitation phenomena in Diesel injector nozzles, Mathematical and computer modelling, 52 (7-8) (2010) 1123-1132.

[16]. F.J. Salvador, S. Hoyas, R. Novella, J. Martínez-López. Numerical simulation and extended validation of two-phase compressible flow in Diesel injector nozzles, Proc. IMechE, Part D: J. Automobile Engineering 225 (2011) 545-563.

[17]. A. Lichtarowicz, R. K. Duggins, E. Markland, Discharge coefficients for incompressible non-cavitating flow through long orifices. J. Mechanical Eng. Sci. 7-2 (1965).

[18]. T.R. Ohrn, D.W. Senser, A.H. Lefèbvre, Geometrical effects on discharge coefficients for plain-orifice atomizers. Atomization Spray. 1(2) (1991) 137-153.

[19]. J.C. Kent, G.M. Brown, Nozzle exit flow characteristics for square-edged and rounded inlet geometries. Combust. Sci. Technol. 30 (1983) 121-132.

[20]. V. Macián, R. Payri, X. Margot, F.J. Salvador, A CFD analysis of the influence of diesel nozzle geometry on the inception of cavitation, Atomization spray. 13 (5-6) (2003) 579-604.

[21]. R. Payri, F.J. Salvador, J. Gimeno, J. De la Morena, Study of cavitation phenomena based on a technique for visualizing bubbles in a liquid pressurized chamber, Int. J. Heat Fluid Fl., 30 (4) (2009) 768-777.

[22]. C. Soteriou, M. Smith, R. Andrews. Direct Injection Diesel Sprays and the Effects of Cavitation and Hydraulic Flip on Atomization. SAE Paper 950080 (1995).

[23]. W.H. Nurick. Orifice cavitation and its effect on spray mixing. ASME J Fluids Eng 681-7 (1976).

[24]. R. Payri, C. Guardiola, F.J, Salvador, J. Gimeno, Critical cavitation number determination in Diesel injection nozzles. Exp. Techniques 28 (3) (2004) 49-52.

[25]. LMS Imagine.Lab AMESim v.8, User´s manual, 2010

LIST OF TABLES

FIGURE CAPTIONS

Figure 12. Complete sketch of the model involving the different parts described.

Figure 13. Model validation at different injection pressures and at different energizing times.

Figure 14. Comparison of the experimental injected total mass with the results of the model.

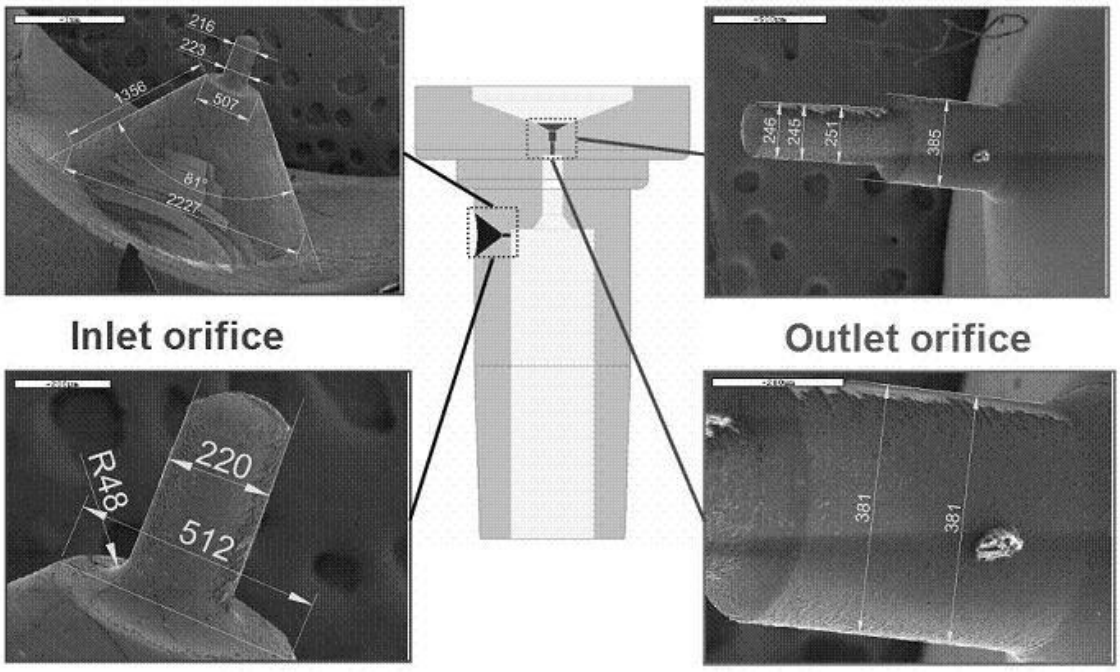

Figure 1. Samples of silicone moulds taken from the injector

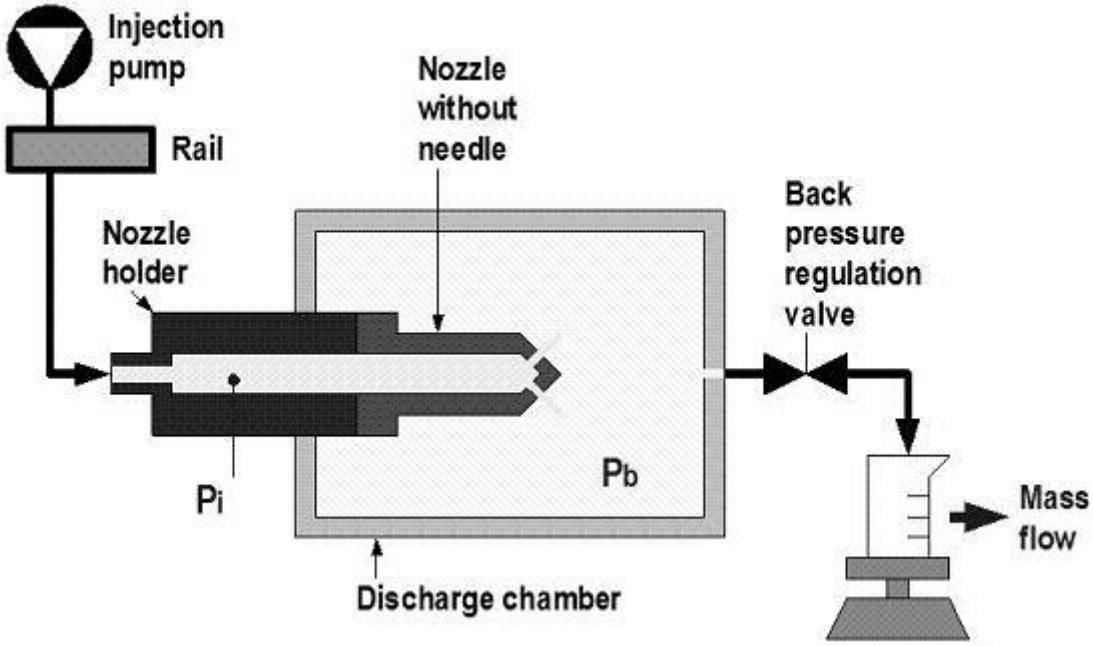

Figure 2. Test rig for the hydraulical characterization of the nozzle.

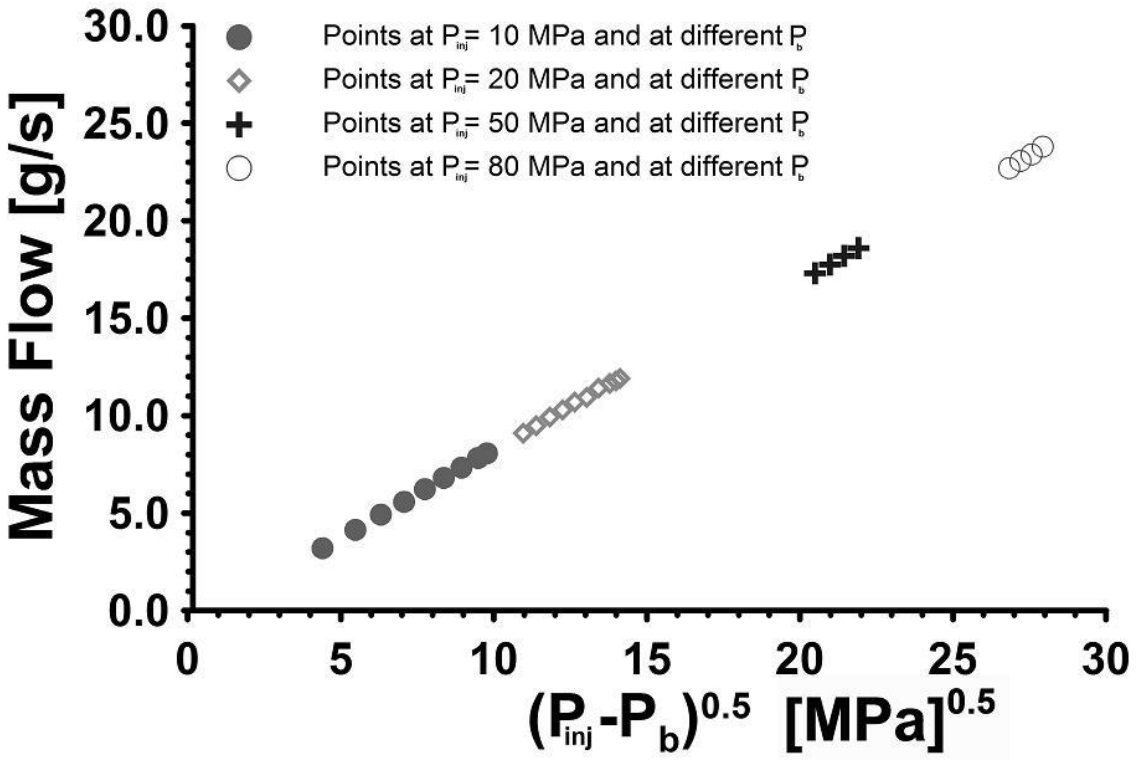

Figure 3. Mass flow against square root of pressure drop for the orifices of the nozzle.

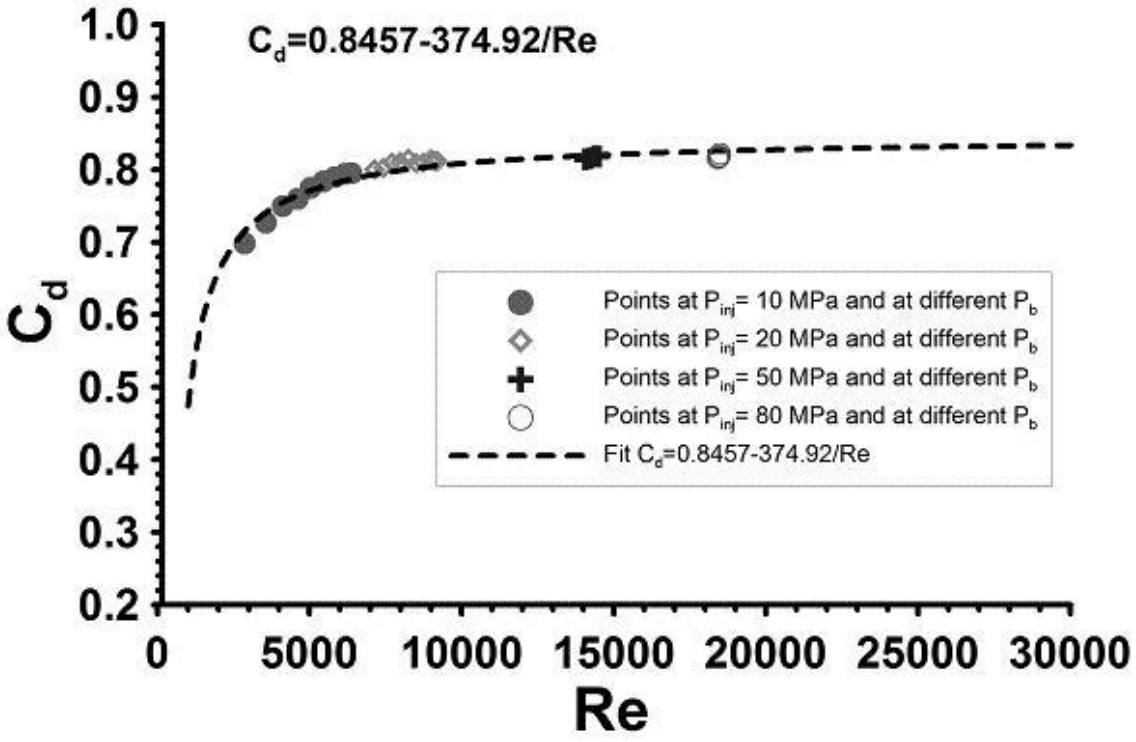

Figure 4. Discharge coefficient of the nozzle against the Reynolds number.

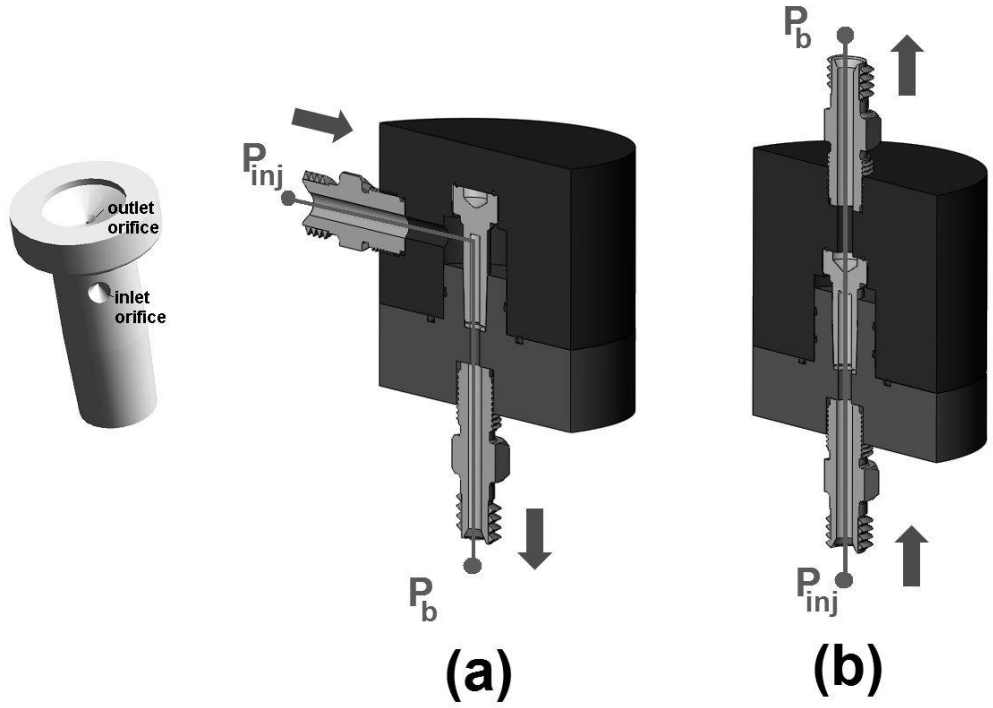

Figure 5. Test rig for the characterization of the control volume orifices.

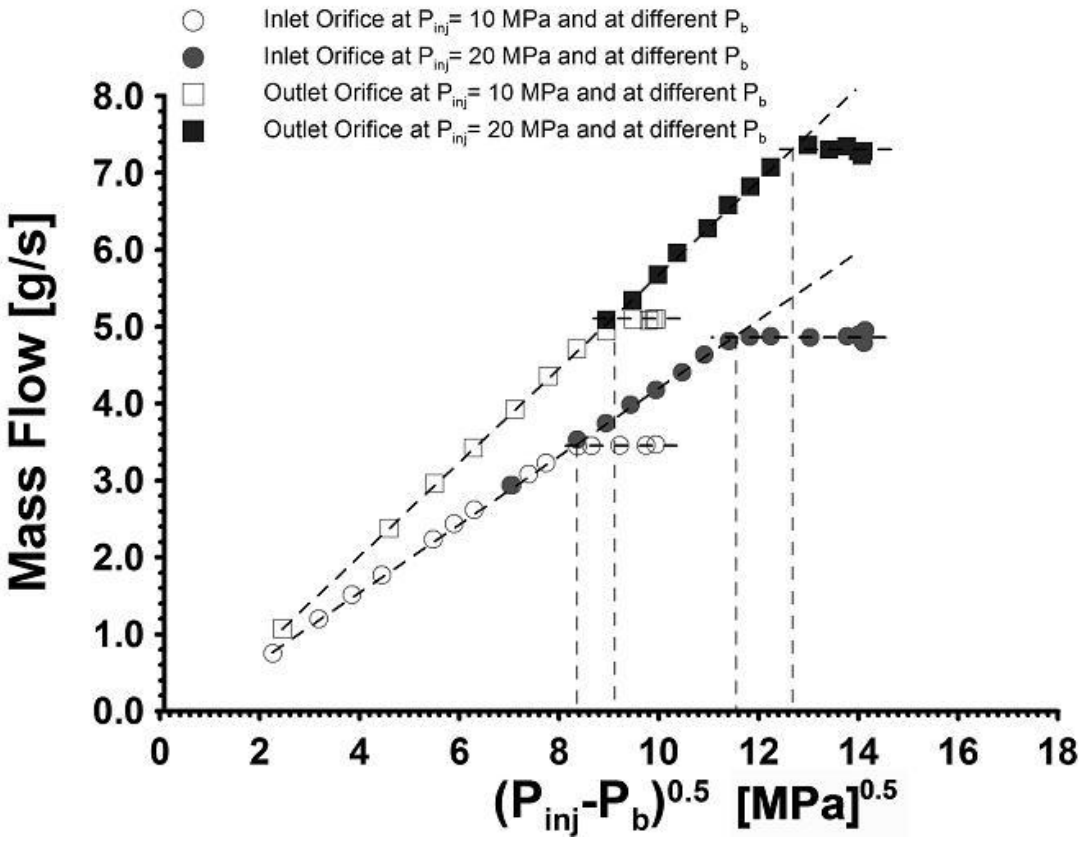

Figure 6. Mass flow against square root of pressure drop for the control orifices.

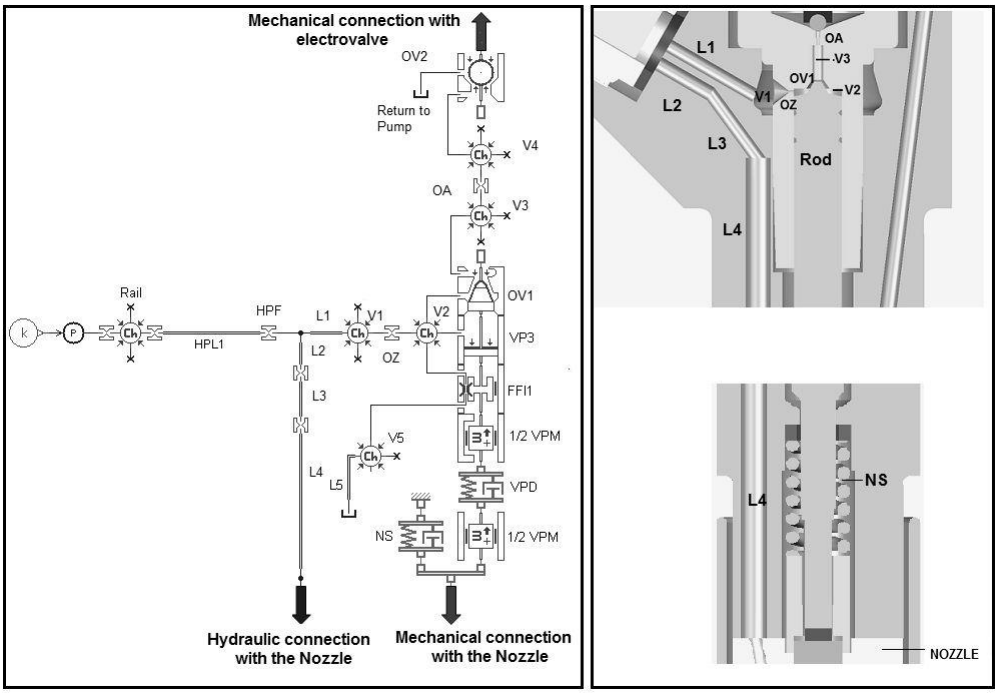

Figure 7. Model of the injector holder.

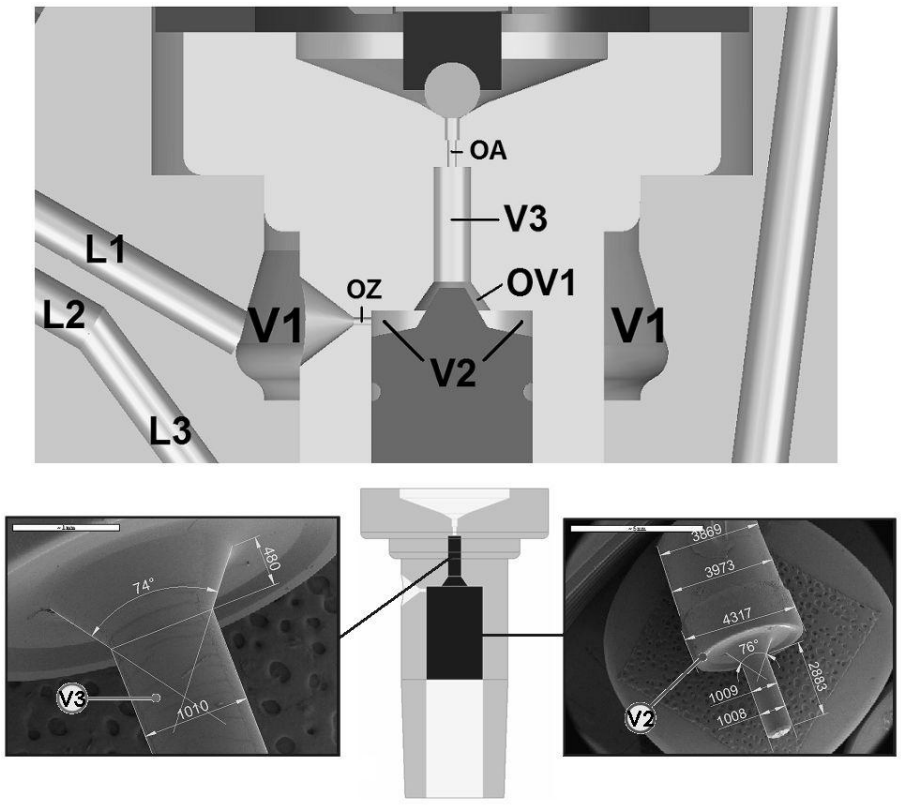

Figure 8. Volumes determination examples.

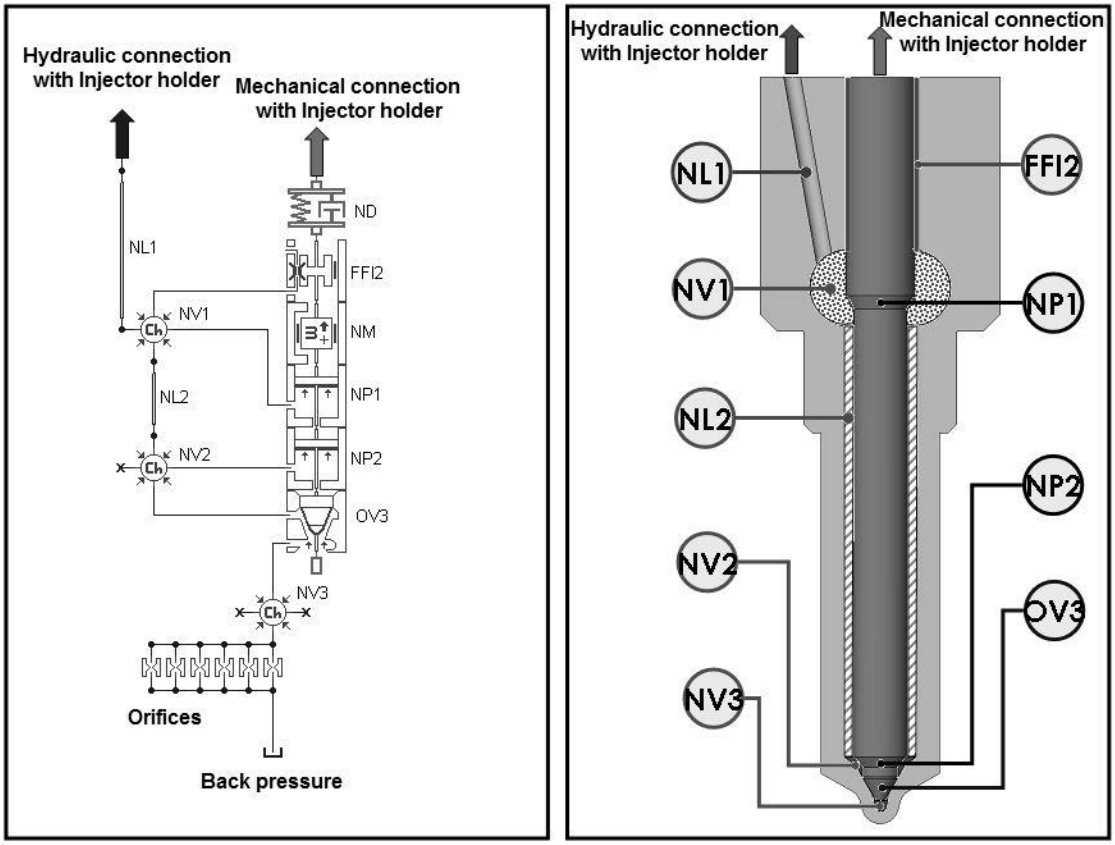

Figure 9. Model of the nozzle.

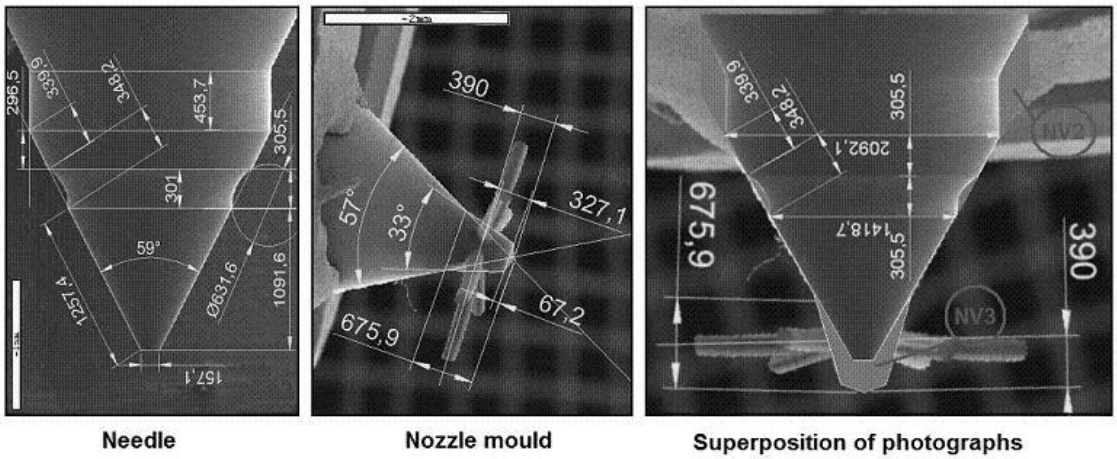

Figure 10. Pictures superposition to characterized volumes in the nozzle.

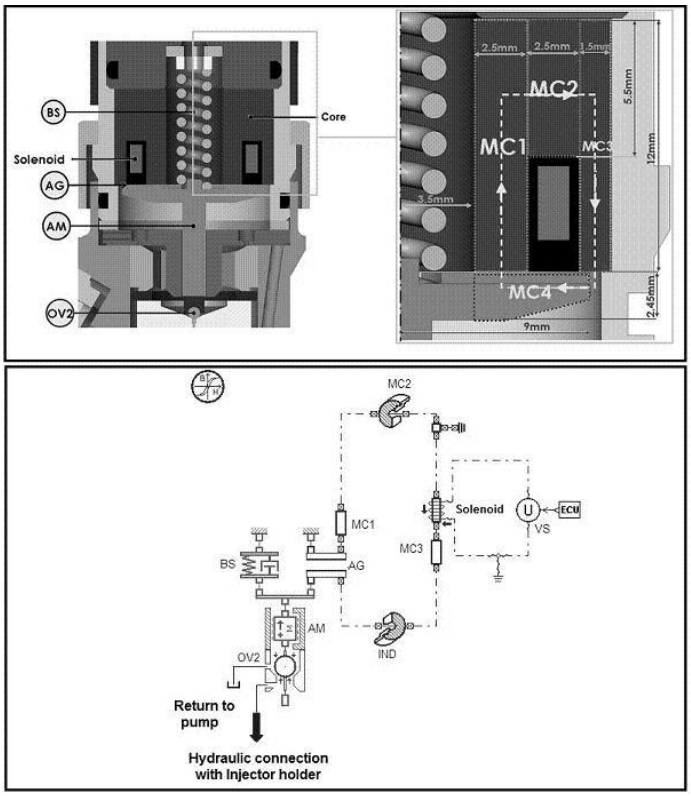

Figure 11. Model of the electrovalve.

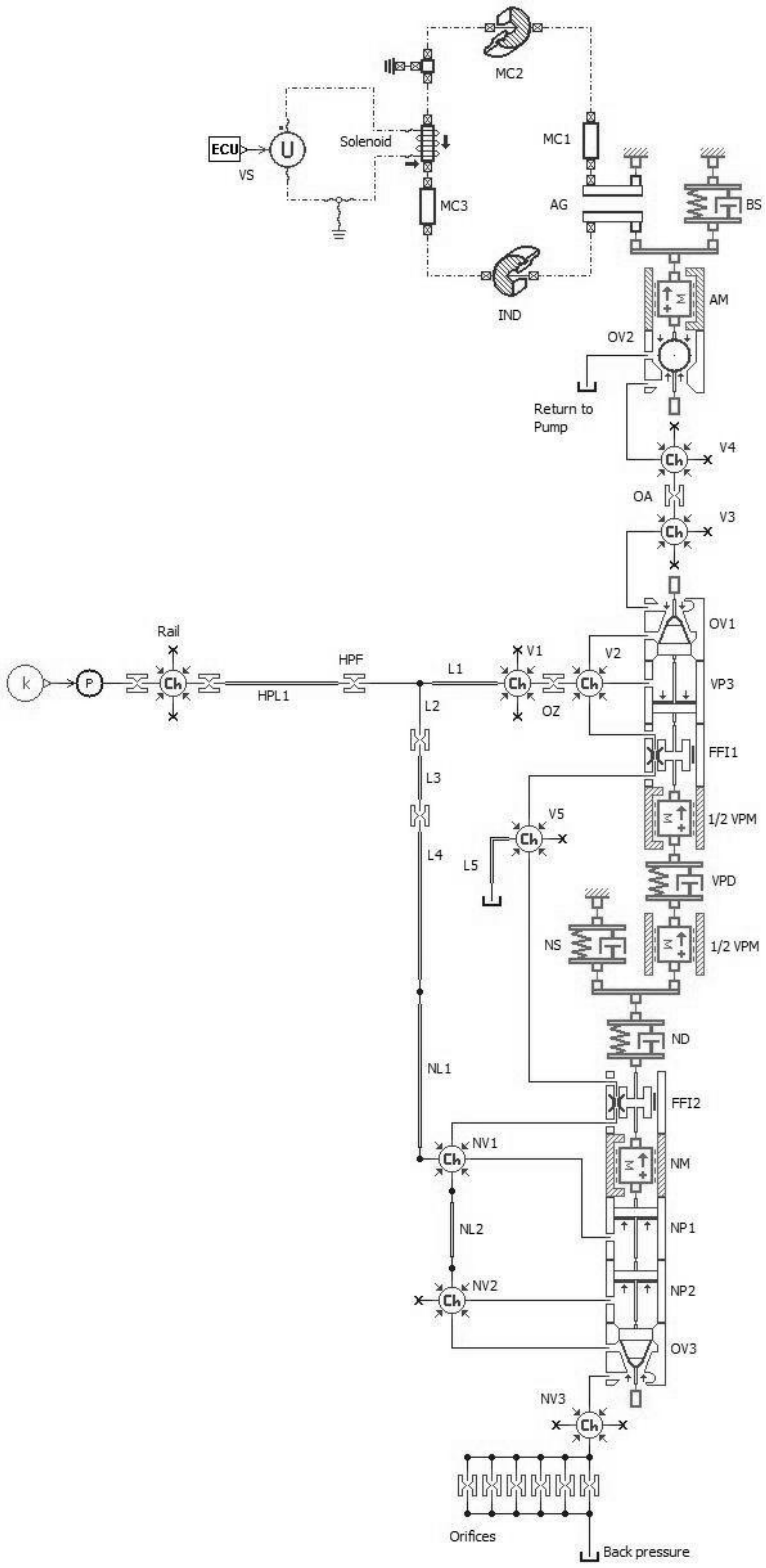

Figure 12. Complete sketch of the model involving the different parts described.

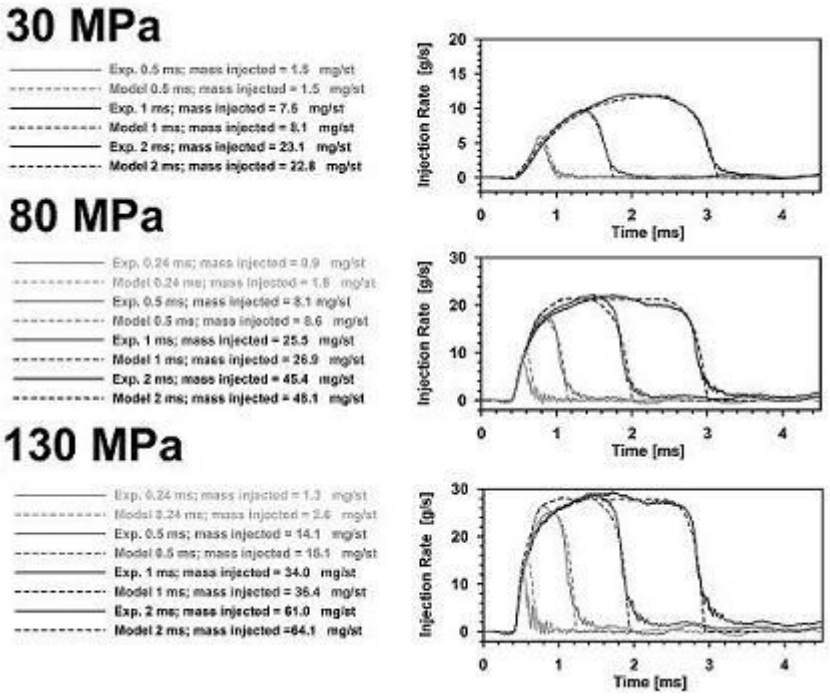

Figure 13. Model validation at different injection pressures and at different energizing times.

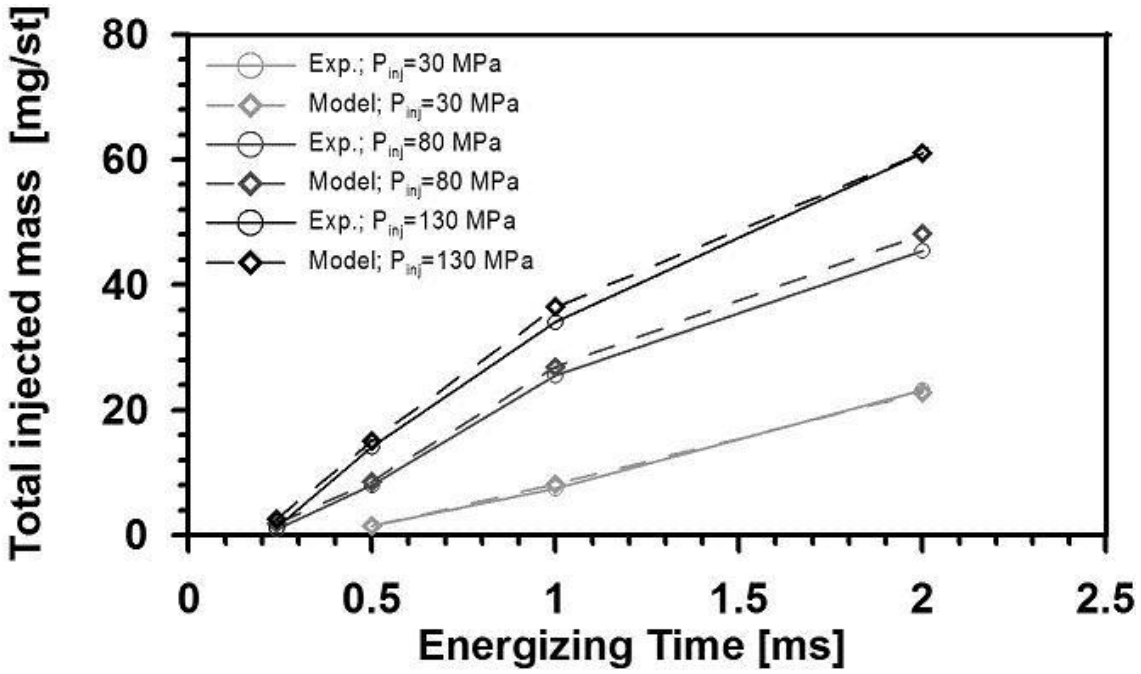

Figure 14. Comparison of the experimental injected total mass with the results of the model.

Table 1. Physical and chemical properties of Repsol CEC RF-06-99 Fuel.

Test	Unit	Result	Uncertainty
Density at 15ºC	kg/m^3	843	±0.2
Viscosity at 40ºC	mm^2/s	2.847	±0.42
Volatility			
65% distillated at	ºC	294.5	±3.7
85% distillated at	ºC	329.2	±3.7
95% distillated at	ºC	357	±3.7
Average fuel molecular composition		$C_{13}H_{28}$	

Table 2. Parameters for the injector holder model

Element	Length (mm)	Diameter (mm)	Volume (cm3)	Mass (g)
OV2	-	0,385	-	-
V4	-	-	5,65E-05	-
OA	-	0,246	-	-
V3	-	-	2.3E-3	-
Rail	-	-	24	-
HPL1	90	2,5	-	-
HPF	1	-	-	-
L1	7,57	1,44	-	-
V1	-	-	0,125	-
OZ	-	0,216	-	-
V2	-	-	0,0115	-
L2	7,22	1,22	-	-
L3	3,39	1,11	-	-
L4	115	2,16	-	-
V5	-	-	0,115	-
L5	58	1,35	-	-
1/2 VPM	-	-	-	6.43
Element	**Spring Rate (N/m)**		**Damper Rating (N/(m/s))**	
VPD	28100000		50	
NS	24093		25	

Table 3. Parameters for the nozzle model

Element	Length (mm)	Diameter (mm)	Volume (cm3)	Mass (g)
NL1	15	2,16	-	-
FFI2	12,6	4	-	-
NV1	-	-	0,032	-
NM	-	-	-	3.1
NP1	-	4	-	-
NL2	27	2,4	-	-
NV2	-	-	0,005	-
NP2	-	3,04	-	-
OV3	-	0,57	-	-
NV3	-	-	5,84E-05	-
Orifices	-	0,13	-	-
Element	**Spring Rate (N/m)**		**Damper Rating (N/(m/s))**	
ND	39330000		50	

Table 4. Parameters for the electrovalve model

Element	Length (mm)	Mass (g)	Area (mm^2)	No. Coils	Resistor (Ohm)
Solenoid	-	-	-	32	0,46
MC1	2x23,32	-	89,34	-	-
AG	0,075	-	86,55		-
AM	-	5.9	-	-	-
Element	**Spring Rate (N/m)**		**Damper Rating (N/(m/s))**		
BS	69000		10		